DOE SBIR Phase I Final Report

D. A. Dimitrov and David L. Bruhwiler
Tech-X Corporation
5621 Arapahoe Ave., Suite A
Boulder, CO 80301

26th May 2005

SBIR Project Title: Advanced 3D Photocathode Modeling and Simulations

DoE Grant Number: DE-FG02-04ER84103

Abstract

High brightness electron beams required by the proposed Next Linear Collider demand strong advances in photocathode electron gun performance. Significant improvement in the production of such beams with rf photocathode electron guns is hampered by the lack of high-fidelity simulations. The critical missing piece in existing gun codes is a physics-based, detailed treatment of the very complex and highly nonlinear photoemission process.

Contents

1 Significance, Background Information, and Technical Approach

In this section, we describe the importance of the software package we proposed to develop. Then, we provide sufficient background information to understand the problem of interest in the context of advanced accelerator research. Finally, we discuss the technical approach we followed.

1.1 Identification and Significance of the Problem or Opportunity

Future advances in fundamental research in high-energy physics require more powerful particle accelerator facilities than those currently in use. The Next Linear Collider (NLC) project [1], still in the conceptual design phase, would accelerate electrons and positrons and collide them at energies high enough to explore limits of the Standard Model and address questions related to the fundamental nature of mass, space and time. A key component of the NLC is the photocathode electron gun [2] that is the subject of on-going R&D [3].

Codes for simulating photocathode electron guns invariably assume the emission of an idealized electron distribution from the cathode, regardless of the particular particle emission model (loading the particles in the simulation) that is implemented. The output data of such simulations, a relatively clean and smooth distribution with very little variation as a function of the azimuthal angle, are inconsistent with the highly irregular and asymmetric electron bunches seen in experimental diagnostics. This is a fundamental problem that must be resolved to facilitate new ideas and designs within the electron gun community leading to the order-of-magnitude performance increase needed by the NLC and other next-generation accelerators.

The opportunity presented by this challenge is to take advantage of recent advances in the theoretical understanding of photoemission from various cathode materials. Our idea is to implement these algorithms in a high-performance 3-D particle-in-cell (PIC) code that is general and flexible enough to accurately model the laser pulse, the emission process, and the subsequent electron beam dynamics. We discuss relevant photoemission models in the background section below and explain algorithms for their implementation in a PIC code in the sections on the tasks we accomplished in the Phase I project. The appropriate PIC code is the VORPAL code [4, 5, 6] under development at Tech-X Corp. and the University of Colorado.

Another application that require significant advances in beam brightness from photocathode electron guns include free electron lasers (FEL), see, e.g., Ref. [7] for an overview of FELs. An FEL of interest to the high-energy physics community is the Linac Coherent Light Source (LCLS) project at the Stanford Linear Accelerator Center (SLAC) [8]. A radio frequency (RF) photocathode electron gun is also under development [9] for the ORION advanced accelerator facility [10] at SLAC.

1.2 Background Information

In this subsection, we discuss relevant background information on electron emission from cathode systems due to different effects and on PIC codes used to model charged particle systems in different high-energy physics (HEP) areas.

1.2.1 Electron Emission

Specific materials become good sources of electrons when interacting with high electric fields, energetic photons, and/or when heated to high temperatures. Cathodes that emit electrons are used in a variety of devices for scientific and commercial applications. Researchers are using and considering designing new photocathodes as sources for linear colliders, free electron lasers, and many other accelerator applications.

The modern designs of photocathodes for HEP applications require beams with higher brightness and current. It is necessary to understand the physics of emission in detail in order to accurately design these advanced characteristics. Predictions from the currently used theoretical models show discrepancies (more than 10%) when compared to measured data, demonstrating that more advanced theoretical models are needed. Moreover, code implementation of computer algorithms based on such realistic models are also needed to provide guidance during the design of advanced photocathodes by quickly exploring different parameter regimes of operation. These simulations will also be very valuable to test the predictions of proposed models when compared to experimental data.

The study of electron emission from cathodes has a long history (over 75 years). A recent account of the theoretical models of field and thermal emission was given by Jensen [11]. The physics of electron emission from cathodes is complicated due to the number of different effects involved (field, temperature, interaction with photons), the nature of the different materials used as cathodes (metals and semiconductors with different material properties), and the treatment and condition (roughness) of the material emitting surface.

Additionally, the electrostatic potential at the emitting surface has multiple length scale contributions. There is a strong dipole layer and many-body effects might have to be considered [11] on an atomic scale at the surface of a cathode. The image charge has to be taken into account on a length scale up to a few microns from a metal cathode. Finally, on a macroscopic scale, there are different potentials associated with dipole layers at different crystal planes that correspond to different crystal plane cuts at the cathode faces.

A quantitative description of photoemission requires quantum mechanics to calculate the probability for transmission of an electron. The time evolution of the electron and ion temperatures of an emitting cathode depend in a complex way on the material properties of the cathode and the intensity of the laser illuminating the cathode surface. It is a difficult task to account for all of these effects.

Recently, a generalized model of electron emission that takes into account field, thermal, and photoemission effects was proposed by Jensen *et al.* [12]. They showed that the model remains correct even in the temperature-field domain where the often used Fowler-Nordheim (FN) and Richardson-Laue-Dushman (RLD) models are no longer applicable. Analysis of a model with electron and lattice temperature relaxation included for different metal cathodes was shown to be in good agreement with experimental data [13, 14]. A theory based on this temperature relaxation approach was developed and applied to metal dispenser cathodes operated in a regime for free electron lasers [15, 16]. However, these advanced theories for photoemission have not been implemented in electromagnetic, particle computer simulation codes.

1.2.2 Particle-In-Cell Codes

The PIC simulation approach was formally described by Birsdall and Langdon [17] and by Hockney and Eastwood [18]. Additions to PIC codes include techniques for handling boundaries, external circuits [19], and Monte Carlo collisions (MCC) with neutral particles [20]. The standard

PIC-MCC scheme solves the equations representing a coupled system of charged particles and fields.

The particles are followed in a continuum space, while the fields are computed on a mesh. Interpolation provides the means of coupling the particles and the fields. The evolution of the particles and the fields at each time step of the PIC simulations is done by first using the forces due to electric and magnetic fields to advance the velocities of the particles. These velocities are then used to advance the positions and then boundary conditions are applied. Next, the particle positions and velocities are used to compute the charge and current densities on the grid.

These densities provide the source terms for the integration of the field equations, the Poisson equation in the electrostatic limit or Maxwell's equations in the electromagnetic limit, on the grid. The fields resulting from the integration are then interpolated to particle locations to calculate the forces on the particles. At Tech-X, we develop and support two PIC codes: the VORPAL plasma simulation framework (the code for which we developed the phothocathode models in Phase I) and the OOPIC 2D PIC code.

1.2.3 The VORPAL Plasma Simulation Framework

Our approach to photocathode and RF gun modeling is to adapt the 3D plasma simulation framework, VORPAL [6], to model plasma formation via laser-matter interaction. The VORPAL code is under development jointly at the University of Colorado and Tech-X Corporation for the purpose of simulating intense laser-plasma physics.

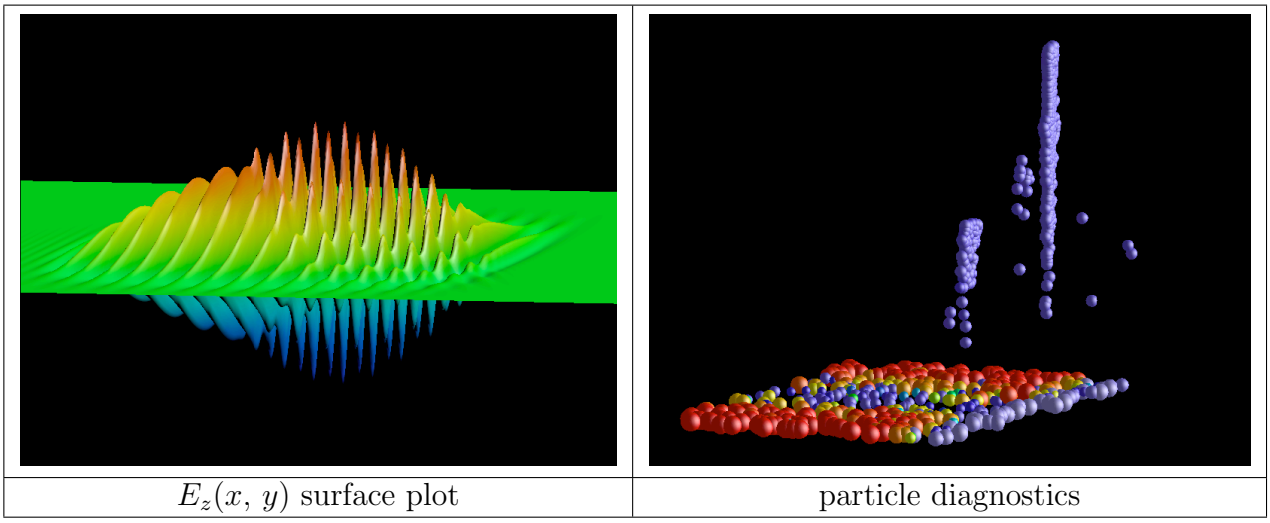

$E_z(x, y)$ surface plot	particle diagnostics

Figure 1: The plot in the left panel demonstrates a visual diagnostic of an electric field component for an oblique collision of two laser pulses generated from VORPAL simulation output data. The right panel shows beams produced through optical injection to a laser wake field. The color and size of the balls indicates the weight of the particles in the simulation. The vertical axis is energy, while the other two axes are longitudinal and transverse position.

The VORPAL framework currently can model the interaction of electromagnetic fields with conducting boundaries, charged particles (of both constant and variable weight), and charged fluids. Included in the fluid implementations are both a cold (pressureless) fluid and a scalar-pressure fluid. The VORPAL framework also has field ionization production of particles, and it

has a Direct Simulation Monte Carlo treatment of neutral and charged fluids, i.e., self collisions for the particle representations.

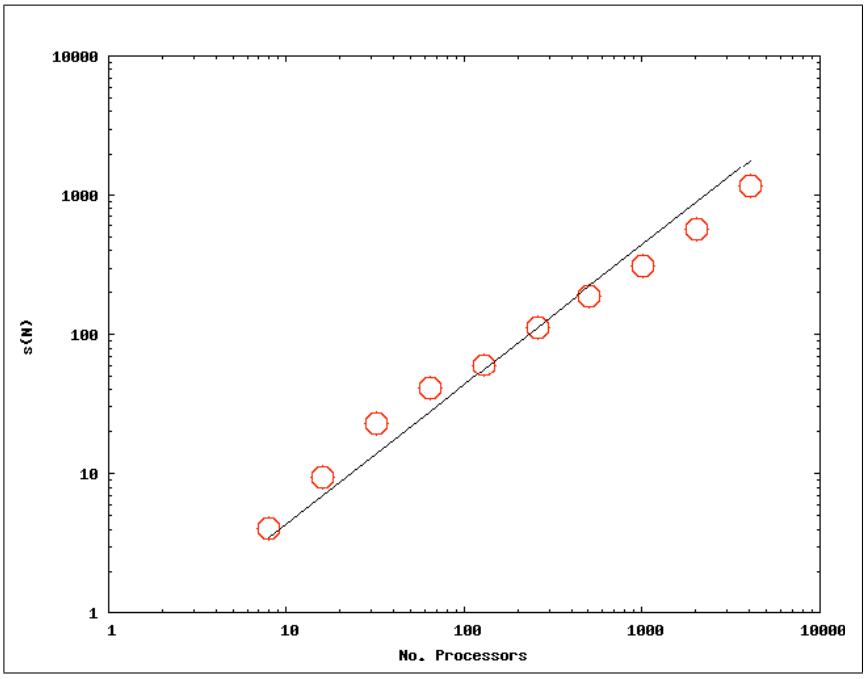

Figure 2: Speedup of VORPAL on the SP3 at the National Energy Research Supercomputer Center.

The VORPAL framework uses C++ templating over both dimension and floating point types, so that one can build 1D, 2D and 3D codes, in both single and double precision, using a single source code base. VORPAL makes use of the templated, reference-counted container classes from the OptSolve++ library [21, 22], which was developed at Tech-X. Output is in the form of Hierarchical Data Format V.5 (HDF5) [23] files, a binary, cross-platform, self-describing data format. In addition, VORPAL was designed to have top-level interaction only through a single object. This will allow VORPAL to be incorporated into a desktop application with a GUI on Windows or UNIX.

The VORPAL framework is designed for use on multiple platforms. Use of the GNU Autotools (automake, autoconf, configure, make, m4) has enabled a VORPAL distribution that can be built and run on Linux and multiple UNIX platforms. In addition, VORPAL has been ported to Windows and Macintosh OS X. VORPAL can run on a parallel Beowulf cluster or on the parallel IBM SP2 through use of the Message Passing Interface (MPI). On OS X, VORPAL works with the LAM MPI implementation. Thus, VORPAL compiles and runs on platforms from desktop CPUs to supercomputers.

VORPAL was designed from the outset to be flexible through use of object-oriented methods. These methods have permitted easy addition of different electromagnetic field solvers, particle dynamics, and charged fluids. For example, VORPAL makes available both an electrostatic solver and an implicit electromagnetic solver. Hence, VORPAL should be easily adapted to include modeling of quasi-neutral hydrodynamics.

Figure 3: Visualization of VORPAL generated data. This visualization of the electron density was created by Cameron Geddes of the Lawrence Berkeley National Laboratory.

At present, VORPAL runs in batch mode, generating output in the form of HDF5 files. The HDF5 self-describing data format supports parallelism via MPI. The files can then be read by any number of visualization tools for further analysis. The VORPAL distribution comes with a number of visualization programs for carrying out this task. Figure 1 shows a visualization of an oblique collision of two laser pulses as simulated by VORPAL and a visualization of a beam of particles in a laser wake-field accelerator.

VORPAL has been shown to scale very well in parallel computations. Figure 2 shows the parallel speedup of VORPAL as a function of the number of processors on the Seaborg machine at the National Energy Research Supercomputer Center (NERSC). The solid line, linear scaling, is very closely followed out to 4000 processors, the maximum number available at NERC. This indicates that VORPAL may be able to make effective use of the even larger number of processors soon to become available at other computing centers.

The VORPAL developers (which now number more than 10) have put together an extensive Web site [4] on how to run and use VORPAL. This Web site includes documentation on the

building and use of VORPAL. The latter includes some preliminary documentation of input files along with documentation on data visualization and run management. The VORPAL modeling application is freely available to the research community under the University of Colorado research license, as noted at the Web site.

Recently, VORPAL has experienced success. Visualization of VORPAL simulation results appeared on the cover of Nature (see Fig. 3). The associated article [24] discusses the production of high-energy particle beams with narrow energy spread through the breakup of laser pulses propagating through a plasma when they are just a bit longer than the plasma wavelength. VORPAL simulations were used to help understand the physics of the experiment.

VORPAL also has capabilities to model fluids. Its scalar pressure fluid model is based on the Euler fluid equations with an ideal gas equation of state. The numerical algorithm used is the Richtmyer predictor-corrector implementation of the Lax-Wendoff method [25]. An adjustable artificial viscosity term was added to the equations so the algorithm could deal with strong shocks.

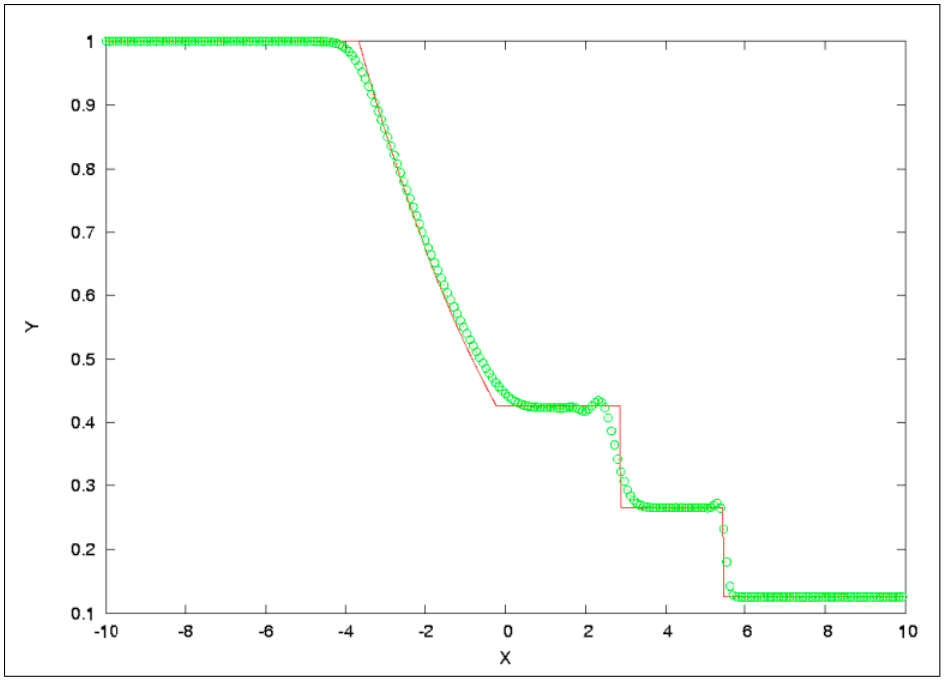

Figure 4: The fluid density plotted versus position for the Sod shock tube. Green circles show results from VORPAL simulation. The red line is the analytical solution. The VORPAL Euler algorithm correctly reproduces the location and amplitude of the shock, contact, and expansion fan.

In Figure 4 we see the fluid density from a VORPAL simulation of the Sod shock tube problem [26] plotted with the analytical solution. The Sod shock tube problem consists of a fluid-filled tube separated into two halves by a membrane. The fluid pressure and density are different in each half. The membrane is then removed instantaneously. At this interface a shock front, contact front, and expansion fan form and propagate. The green circles in Figure 4 are the results from VORPAL and the red line is the analytical solution. VORPAL reproduces the location and shape of the all three features of the Sod shock problem.

1.3 Technical Approach

Our overall technical approach consisted in implementing advanced physics models for electron emission from cathodes taking into account field, thermal, and photoemission effects using the multidimensional VORPAL code. Our algorithm development and code implementation is based on the recent theoretical models developed by Jensen *et al.* [15, 12, 27]. We worked with Prof. Patrick G. O'Shea's group in the Institute for Research in Electronics & Applied Physics at the University of Maryland and Dr. Kevin Jensen from the Naval Research Lab during Phase I development. We will continue to work in close collaboration with them, as well as with Dr. John Lewellen from the DoE Argonne National Lab, during the Phase II.

Our overall technical approach for the Phase II project is to:

1. verify the VORPAL code with 3D simulations by comparison with other RF gun codes and with analytical calculations,
2. validate our results by comparison with experimental results from Prof. P. O'Shea's group in University of Maryland and from Dr. John Lewellen from Argonne National Lab
3. make available, through VORPAL, a suite of advanced photoemission models for dispenser cathodes, including models for emission by very short laser pulses,
4. extend VORPAL to enable full 3D RF gun simulations with it,
5. use VORPAL to simulate RF gun systems of current research interest to investigate the predictive capabilities of the implemented models and provide feedback to on-going experimental studies in the field (in collaboration with Prof. O'Shea, Dr. Kevin Jensen, and Dr. J. Lewellen),
6. develop a stand-alone software library with these models for direct use with other codes.

Moreover, we will use our physics and computer science experience to implement and document the package for interoperability with the main programming languages used to develop PIC codes and for portability across different combinations of hardware and operating systems software.

2 Phase I Accomplishments

We successfully solved all of the Phase I project problems. These results prove the feasibility of the proposed approach. The work done in Phase I built a sound foundation for the development of a complete prototype in Phase II of the project. What is most exciting is the unique opportunity these models will provide in VORPAL for the most realistic modeling of RF photocathode guns with a particle-in-cell code currently available. We consider each of the Phase I tasks now and describe how we accomplished them.

2.1 Task 1: Implement a detailed photoemission algorithm in VORPAL

This was the main Phase I task to be accomplished. It required the implementation of not only an advanced physics model for a photocathode but also the development of the overall VORPAL code infrastructure to support simulation of RF gun photocathode devices.

Algorithm 1 shows the pseudo code for the high-level representation of our implementation in VORPAL. It represents the large-scale logic for running an RF gun photocathode simulation with VORPAL.

Algorithm 1 RF Gun Photocathode Simulation

```
// During VORPAL initialization:
...
// Instantiate photocathode emitter and dispenser cathode objects:
new VpPhotocathodeEmitter<FLOATTYPE, NDIM>
  new VpDispenserCathode<FLOATTYPE, NDIM>
// Initialize the new emitter/cathode objects with their input file parameters:
VpPhotocathodeEmitter<FLOATTYPE, NDIM>::setAttrib(inpFileAttribs)
  VpDispenserCathode<FLOATTYPE, NDIM>::setAttrib(inpFileAttribs)
...
for i ← 1 to N_t do
  // During VORPAL time step update:
  ...
  VpPhotocathodeEmitter<FLOATTYPE, NDIM>::loadParticles(slab)
  ...
end for
```

We wrote two major C++ classes (objects) to handle the tasks for managing the emittance from the photocathode and for the actual calculation of the steady state physics model given in Ref. [15]. The handling of electron emission from a photocathode is done in the VpPhotocathodeEmitter<FLOATTYPE, NDIM> class.

The syntax of this class name follows the C++ programming language template syntax. It allows a C++ class author to define objects that use data of different types in the same code base but writing the source code for each of these common objects just once. In the case of VORPAL, we use the C++ template mechanism to write a single source code base that can be executed in double and/or single precision (depending on the value of the FLOATTYPE type name) and for 1D, 2D, and 3D simulations. This is extremely general and flexible for the users of the code but requires more work on the side of the VORPAL code developers. Text on a line in Algorithm 1 starting with "//" is a comment that extends to the end of the line.

The VpDispenserCathode<FLOATTYPE, NDIM> implements the physics model for the calculation of the steady state approximation for the cathode photo and thermal currents as given in Ref. [15]. Jensen *et al.* applied this model to investigate emission from a dispenser cathode. The value of the FLOATTYPE template parameter is set at run time using the data in the VORPAL input file. It allows users to select double or single precision of execution depending on precision and computational requirements.

We designed the code to instantiate the photocathode emitter and dispenser cathode objects only if the data in a VORPAL input file request a simulation with a photocathode. Once the objects of these two types are initialized, the actual loading of electrons emitted from a photocathode happens at each time step. It is done in the loadParticles(slab) member function of the VpPhotocathodeEmitter object provided the emission current is nonzero.

The pseudo code for the loadParticles(slab) member function of the VpPhotocathodeEmitter object is shown in Algorithm 2. The slab argument that is passed to this function is an orthogonal parallelepiped domain in 3D with one of its surfaces corresponding to the surface

Algorithm 2 loadParticles(slab)

```
if slab has zero volume then
  return
end if
N_cells ← number of photocathode emitter cells
X_cells[N_cells] ← position vectors of photocahode
for i ← 1 to N_cells do
  E ← electric field magnitude in cell i
  I ← laser intensity at location vector X_cells[i]
  J ←VpDispenserCathode<FLOATTYPE, NDIM>::getSteadyStateJ(T_B, E, I)
  N_macro ← getNumberMacroParticles(J)
  for j ← 1 to N_macro do
    t_m ← (quasi) randomly chosen value in [0, dt]
    x_m ← random location on surface of cathode in j^th cell
    // set the macro particle velocity according to acceleration in the E field over time t_m
    v_m ← getVm(t_m, E)
    Δx_m ← macro particle displacement over t_m
    addParticleCurrentToFieldSource(x_m, v_m, t_m, Δx_m)
    x_m ← x_m + Δx_m
    addParticle(x_m, v_m)
  end for
end for
return
```

of the photocathode material. The slab parameters are specified in the section of a VORPAL input file for the definition of the photocathode emitter object.

If the slab has non zero volume, the algorithm proceeds to calculate the photo and thermal currents for each simulation cell on the surface of the cathode. The magnitude of the electric field for the cell is needed (its direction is also checked; if it is a decelerating field, no particles are emitted from the cell) and the intensity of the impacting laser pulse as well. After these are calculated, the evaluation of the electron current density from the steady state model [15] is done in the member function getSteadyStateJ(T_B, E, I) of the VpDispenserCathode<FLOATTYPE, NDIM> object. The first argument of this function is the photocathode bulk temperature.

The algorithm proceeds by calculating the number of macro particles to be emitted from the cell. This number is determined from the total charge to be emitted given the calculated thermal and photo current density J and the charge per macro particle specified in the input file (which must be picked carefully to reduce the numerical noise in the simulations). Finally, the macro particles are deposited in the VORPAL simulation domain and their associated currents during the emission are added to the field sources.

The deposition of each particle was done using the following basic algorithm. Each macro particle is considered emitted from a random location on the photocathode surface cell and at random time $dt - t_m$, $0 \leq t_m \leq dt$, during a VORPAL simulation time step interval. Once this time and location are set, the macro particle is accelerated in the external field over the time interval t_m to determine its final location, deposition velocity, and displacement.

We implement a calculation for the emitted current density (the total of the photo and

thermal current densities) in the GETSTEADYSTATEJ(T_B, E, I) function using the expression given by Eqn. (14) in Ref. [15]:

$$\begin{aligned} J_\lambda\left(T_e,\,\Phi\right) &= q\left(1-R\right)\frac{I_\lambda\left(t\right)}{\hbar\omega}\left(\frac{U\left(\beta\left(\hbar\omega-\phi\right)\right)}{U\left(\beta\mu\right)}\right)+J_{RLD}\left(T_e,\,\Phi\right), \\ J_{RLD}\left(T_e,\,\Phi\right) &= A_{RLD}T_e^2\exp\left(-\beta\phi\right), \end{aligned} \tag{1}$$

where q is the electron charge, T_e is the electron temperature, $\beta = 1/k_B T_e$ with k_B the Boltzmann constant, Φ is the work function (the difference between the potential barrier maximum and the chemical potential at zero field), and $\phi = \Phi - \sqrt{4QF}$ is the effective potential barrier maximum when the image charge potential and the external electric field are considered [11]. The image charge factor is denoted by Q, F is the magnitude of the electric field, and $\sqrt{4QF}$ is the Schottky barrier lowering. The current density $J_{RLD}\left(T_e,\,\Phi\right)$ is calculated in the Richardson approximation for the electron transmission probability; the transmission probability is unity when the electron energy E is greater than the photocathode barrier height $\mu+\phi$ (μ is the chemical potential) and zero otherwise, i.e. $T(E) = \theta(\mu+\phi-E)$ where $\theta(x)$ is the Heaviside step function. This is a classical mechanics description of the transmission. The coefficient $A_{RLD} \approx 120$ A/cm^{2}T^2 is the Richardson constant [11]. The laser intensity interacting with the photocathode surface at time t is $I_\lambda\left(t\right)$, R is the fraction of the reflected laser light, $\hbar\omega$ is the energy of the incident photons with a wavelength λ, and $U\left(x\right)$ is the function

$$U\left(x\right) = \int_{-\infty}^{x} \ln\left(1+e^y\right) dy. \tag{2}$$

Note that the Richardson approximation for the electron transmission probability is a significant simplification which restricts the parameter domain of the model applicability. We will consider emission models based on a generalization [12] of the Richardson-Laue-Dushman (RLD), the expression for the J_{RLD} current in Eq. (1), and the Fowler-Nordheim (FN) equations during Phase II. This generalized model can be applied under extended physical conditions that are of importance in high-energy physics. Under such extreme conditions, the RLD and FN equations are often no longer applicable. The current density of the generalized electron emission model has the RLD and FN equations as asymptotic limits. The transmission probability is also treated quantum mechanically to account for tunneling.

The main problem when calculating the current density from Eqn. (1) is to determine the electron temperature that enters in it. T_e depends generally on time and position in the photocathode and is coupled to the ion (lattice) temperature T_i. We investigate the general equations for the electron and lattice temperature relaxations in the next task. Here, we consider a number of approximations [15] that lead to an *analytic* solution of the coupled equations for T_e and T_i.

For specific cathodes and experimental conditions, the time scale of the laser pulse used is much larger than the electron-electron τ_{e-e} and electron-phonon τ_{e-ph} relaxation times. For a time step in PIC simulations that resolves the laser pulse, but is much larger than τ_{e-e} and τ_{e-ph}, the electron and lattice temperatures will be in equilibrium (a steady state approximation). This is the case for laser pulses with time scale of the order of 10 ps and metal photocathodes with τ_{e-e} and τ_{e-ph} of the order of 0.1 ps [15].

Moreover, if the electron temperature dependence on the spatial coordinate axis z (perpendicular to the emitting surface) is approximated with a decreasing exponential function (i.e. T_e decreases exponentially from its value at the emitting surface, $z = 0$, to its bulk value) and the

electron gas heating is approximated using bulk photocathode material parameters, then it can be shown [15] that the electron temperature at the cathode surface is a solution of the equation

$$T_e^2 \left(T_e - T_0\right) = \frac{3n^2 G(z=0,\, t)}{\gamma \left(B_{e-ph} + A_{e-e} T_0\right)}. \tag{3}$$

$T_e \equiv T_e(z=0)$ is the definition used in this equation while T_0 is the electron bulk temperature. The $G(z=0,\, t)$ is a function of the laser intensity and is defined below by Eq. (8), $\gamma \equiv C_e(T_e)/T_e$ where $C_e(T)$ is the electron heat capacity, and the factor n is of the order of the laser pulse time scale over the electron scattering time scale squared. The B_{e-ph} and A_{e-e} are photocahode material dependent coefficients entering in the equations for the relaxation times at high temperatures (see, e.g., Ref. [13] and the references therein)

$$\tau_{e-e}\left(T_e\right) = \frac{1}{A_{e-e} T_e^2}, \tag{4}$$

$$\tau_{e-ph}\left(T_i\right) = \frac{1}{B_{e-ph} T_i}. \tag{5}$$

Note that in the steady state approximation used in this task, the ion and electron temperatures in Eqns. (4) and (5) are equal at each time step.

We designed the VpDispenserCathode object to solve this steady state model for the electron and ion temperatures and then to calculate the total photocathode current density using the electron temperature. The implementation of this object provides all auxiliary functionality in order to manage the calculation of the electron temperature and the photocathode current. This includes initialization of all photocathode solid state physics parameters, a solver for the cubic equation for T_e, the electron specific heat, the $G(z=0,\, t)$ and $U(x)$ functions. We discuss results from simulations of beam emittance from a Cu photocathode in an RF gun in the description of Task 3 of this Phase I Final Report.

2.2 Task 2: Prototype code for photoemission by shorter laser pulses

In this task, we developed proof-of-principle code for the time dependent temperature evolution of a photocathode electron and ion subsystems. This capability is required to model photoemission due to shorter (pico- and subpicosecond) laser pulses. Subpicosecond laser pulses are necessary for high-frequency RF photocathode guns For example, X-band frequencies are being considered for many future projects, including the NLC. The fully developed prototype of this code will be implemented in VORPAL in Phase II.

During the writing of the Phase I proposal, we envisioned to develop the proof-of-principle code for this task outside of VORPAL. Our reasoning was motivated by the need for as quick as possible code development for this new idea given the very limited Phase I time and resources. We planed to use an interactive development environment for quick code prototyping, such as the Python programming language, rather than the compile-link-debug C++ development cycle we do with VORPAL.

After the work we did in the previous task, it became clear that all the infrastructure code for modeling of photocathodes has to be reimplemented again in Python to support the interactive development approach. It was clear that it was better to reuse as much as possible the VORPAL C++ code developed in Task 1 rather than reimplementing the supporting code base in Python before moving to the new code development. Thus, we proceeded to investigate the solution

of the time dependent temperature equations in VORPAL. However, this code was developed only for the particular case of a Cu cathode for the purpose of finding of a feasible approach and without any extensive error handling. The generalization of this experimental code, its verification and validation, represent a major part of the Phase II project.

For subpicosecond pulses, the calculation of the emission current requires the determination of the electron and ion temperatures from a direct solution of the system of coupled nonlinear partial differential equations for T_e and T_i [13, 15] (attributed to Anisimov *et al.* [28])

$$C_e \frac{\partial T_e}{\partial t} = \frac{\partial}{\partial z}\left(k\left(T_e,\, T_i\right)\frac{\partial T_e}{\partial z}\right) - g\left(T_e - T_i\right) + G\left(z,\, t\right), \tag{6}$$

$$C_i \frac{\partial T_i}{\partial t} = g\left(T_e - T_i\right). \tag{7}$$

C_e and C_i are the electron and ion heat capacities and $k\left(T_e,\, T_i\right)$ is the electron thermal conductivity. The amount of energy transfered by the electrons to the lattice per unit time and volume is given by $g\left(T_e - T_i\right)$ where g is a parameter that depends on the photocathode material properties [13, 15]. The amount of laser pulse power density absorbed by the photocathode is represented by the $G\left(z,\, t\right)$ function

$$G\left(z,\, t\right) = \left(1 - R\right) I_\lambda\left(t\right)\left(\frac{e^{-z/\delta}}{\delta}\right)\left(1 - \frac{U\left(\beta\left(\hbar\omega - \phi\right)\right)}{U\left(\beta\mu\right)}\right), \tag{8}$$

where δ is the photocathode penetration depth of the incident photons. Only the temperature relaxation along z is considered since often in experiments the heat diffusion along z dominates over the diffusion in the plane of the emitting cathode surface. This is usually the case when the laser focal diameter is sufficiently large [13].

The electron temperature (6) is modeled using the heat diffusion equation [29]. The system of partial differential equations, Eqs. (6) and (7), is nonlinear due to the dependence of the electron thermal conductivity on T_e. In 3D, the first term in this equation becomes $\bigtriangledown \cdot \left(k\left(T_e,\, T_i\right) \bigtriangledown T_e\right)$. However, the diffusion along the emitting surface could often be neglected, as is discussed in Refs. [13, 15] and considered here as well.

The numerical algorithm we implemented for the solution of the coupled partial differential equations, Eq. (6) and Eq. (7), is based on a predictor-corrector implicit-explicit (Crank-Nicolson's method) finite difference numerical scheme suggested by K. Jensen *et al.* [27]. This method is accurate to second order in both time and space [30, 31].

We solved these equations with the following initial conditions:

$$T_e\left(z,\, t = 0\right) = T_i\left(z,\, t = 0\right) = T_{bulk}. \tag{9}$$

Boundary conditions are imposed on the electron temperature T_e and T_i. We considered a simulation domain along the direction z, perpendicular to the surface of the cathode, in the interval $z_0 \leq z \leq 0$, $z_0 < 0$. The surface of the cathode is at $z = 0$. Negative values of z are for points inside of the photocathode material. We impose an absorbing boundary condition at z_0:

$$T_e\left(z = z_0,\, t\right) = T_{bulk}, \tag{10}$$

and a reflecting boundary condition at the photocathode surface (no temperature flux across it):

$$\frac{\partial T_e}{\partial z}\left(z = 0,\, t\right) = 0. \tag{11}$$

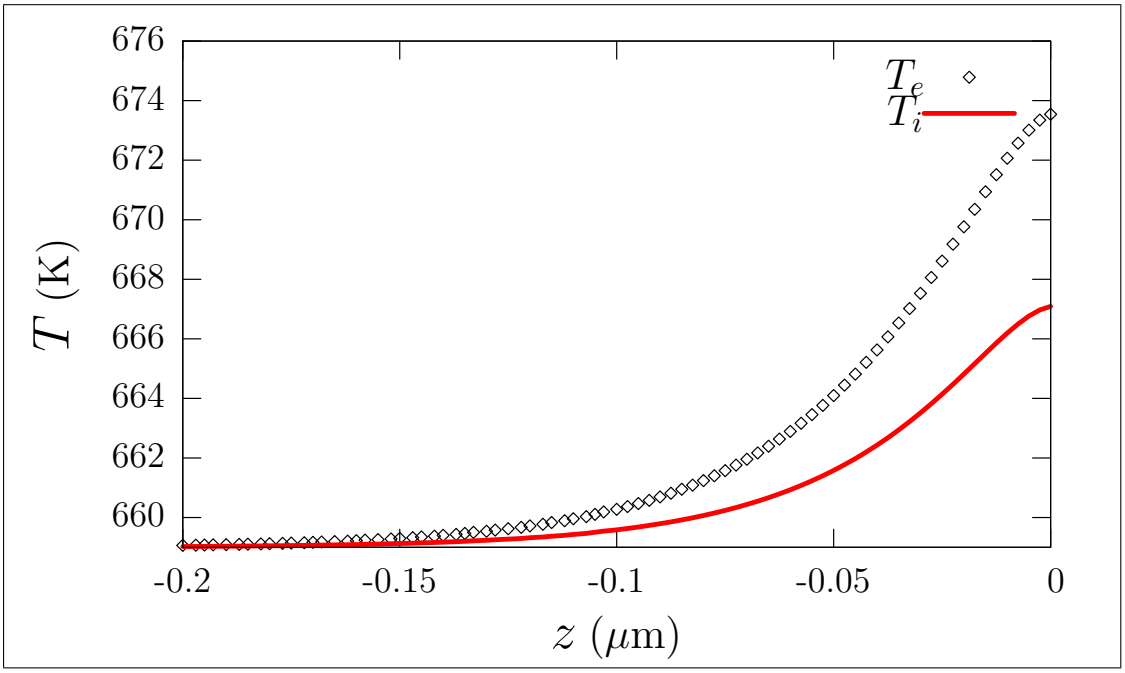

Figure 5: Electron and lattice temperatures from the PDE solution.

Note that in more than one spatial dimension the reflecting boundary conditions is $\mathbf{n}\cdot \nabla T_e|_{(z=0,\,t)} = 0$, where $\mathbf{n}$ is a vector normal to the surface. The same boundary conditions are imposed on the lattice temperature T_i too.

We tested the implemented solver on a Cu photocathode with a Gaussian laser pulse intensity envelope interacting with the cathode. The laser pulse intensity envelope is centered at 3 longitudinal rms (standard deviations) from the surface of the cathode at $t = 0$. It starts to propagate in a direction normal to the photocathode surface. The analytical form of the laser envelope is discussed in detail in the presentation of the next task. The solid state physics parameters for the Cu photocathode are presented in Table 1. The time step used for the solution of the system of partial differential equations was $dt \approx 0.1$ ps and the space step was $dz = 2.5$ nm. The initial temperature of the photocathode was $T_{bulk} = 659$ K.

The solution for the electron and ion subsystem temperatures along the line perpendicular to the photocathode surface and parallel to the line through the center of the laser pulse (along its direction of propagation) is shown in Fig. 5. This is the solution at $t \approx 13$ ps. This time approximately corresponds to the the time the maximum of the laser pulse intensity envelope reaches the surface of the photocathode, i.e. during the time interval $0 \leq t \leq 13$ ps of the simulation, half of the pulse has reached the photocathode surface and interacted with it. The behavior is as expected: the electron and ion temperatures are at their highest values at the surface of the cathode and then decrease to the bulk value when into the cathode material. In this region, the electron and ion subsystems are out of equilibrium with the electron temperature being higher than the ion temperature.

These results indicate that the time dependent model has the potential to provide the most accurate and advanced description of the photocathode thermal effects and thus the emitted current which is strongly dependent on the electron temperature. The main code development work during the Phase II project is focused on developing a complete and robust prototype for this model model.

2.3 Task 3: Validation of VORPAL simulations

Our goal in this task was to simulate specific photocathode emission parameters to test the implementation of the model described in the Phase I Task 1. We investigated different numerical approaches to spatially distribute emitted electron macro particles and their velocities in the first cell layer over the photocathode in the PIC simulations. The results discussed below are based on the algorithm we chose and implemented for the loading of macro particles, Algorithm 2. This algorithm can be extended in a number of ways, e.g. by distributing the macro particles with additional thermal velocity. These extensions are part of the work planned for Phase II.

We also considered the treatment of the emission along the surface of the emitting photocathode boundary due to the different transverse laser intensities at the different boundary computational cells. The laser pulse interacting with the photocathode was modeled by an intensity envelope with Gaussian functional forms along each direction in 3D. The analytical form of laser pulse intensity profile is given by

$$I = I_0 \exp\left(-2\frac{x^2}{l_x^2} - 2\frac{y^2}{l_y^2}\right) \exp\left(-2\left(\left(t - t_0\right)c + \left(z - z_0\right)\right)^2 / l_z^2\right), \tag{12}$$

and can also be written in the form

$$I = I_0 \exp\left(-2\frac{x^2}{l_x^2} - 2\frac{y^2}{l_y^2}\right) \exp\left(-2\left(t - t_0^{eff}\right)^2 / \left(\Delta t\right)^2\right),$$

with $l_z = c\Delta t\sqrt{2}$ and $l_\alpha^{\mathrm{rms}} = l_\alpha/2$ for $\alpha = x,\, y,\, z$. This analytical form describes a laser pulse intensity envelope centered at $(0,\, 0,\, z_0)$ spatially at the beginning of a VORPAL simulation $t = t_0 = 0$.The position z_0 was chosen to be 3 rms pulse lengths, $3l_z^{\mathrm{rms}}$ from the surface of the photocathode. The numerical parameters for the laser pulse envelope used in the simulation results presented in here are given in Table 1. These are parameters that are relevant to photocathode RF gun experiments and are also simulated by others in the field [32, 33].

Symbol	Definition	Value	Units
λ	laser pulse wavelength	266.0	nm
l_z	effective z pulse length	2.54382336	mm
l_x	effective x pulse length	3.33333333333	mm
l_y	effective y pulse length	3.33333333333	mm
Δt	effective pulse time	6.0	ps
E_0	RF field magnitude	50.0	MV/m
ν_{rf}	RF field frequency	1.3	GHz
ϕ_0	RF field phase	248.086664951	degrees
T_0	Initial photcathode temperature	659.0	K
N_A	absorbate material atomic #, -1 for none	-1	-
N_B	bulk material atomic #, -1 for none	29	-
E_{EF}	field enchancement factor	1.0	-
μ	chemical potential	7.0	eV
η	thermal mass factor	1.375	-
Φ	absorbate material work function	0.0	eV
Φ_W	bulk material work function	4.6	eV
A_0	e^- - e^- relaxation time parameter	25.1	-
λ_0	e^- - phonon relaxation time parameter	0.2261	-
υ_s	Cu sound velocity	476000.0	cm/s
T_D	Cu Debye Temperature	347.0	K
ρ_0	Cu density	8.96	g/cm^3
n_0	Cu number density	8.49e+22	cm^3
δ	Cu photon skin depth	10.4158	nm
R	Cu Reflectivity	0.942309	-
θ	cathode coverage (by absorbate material) factor	0.0	-
n	cathode temperature decrease length factor	17.321	-
L_z	simulation box length along z	22.89441024	mm
L_x	simulation box length along x	30.0	mm
L_y	simulation box length along y	30.0	mm
N_z	# of cells along z	600	-
N_x	# of cells along x	150	-
N_y	# of cells along y	150	-
dt	simulation time step	1.16740593862e-13	s
I_0	laser pulse intensity magnitude	10.237116293	MW/cm^2
$\|Q_{beam}\|$	charge of emitted beam	0.505877992817	nC

Table 1: Selected parameters automatically extracted from a VORPAL input file (except for the total beam charge, the last parameter in the table, which was calculated from the raw simulations data after the beam was completely emitted) for 3D simulations of electron beam generation from a Cu photocathode in an RF gun.

The analytical form of the RF field we used in the simulations can be expressed in cylindrical

coordinates via the equations

$$\begin{aligned} E_z &= E_0 \cos(kz) \sin(\omega t + \phi_0), \\ E_r &= E_0 \frac{kr}{2} \sin(kz) \sin(\omega t + \phi_0), \\ B_\phi &= E_0 \frac{kr}{2c} \cos(kz) \cos(\omega t + \phi_0), \end{aligned} \tag{13}$$

where $\omega = 2\pi\nu_{rf}$, $k = \omega/c$, andν_{rf} is the RF field frequency. We converted E_r and B_ϕ in Cartesian coordinates in the representation of the RF field in VORPAL. The RF field is specified with its analytic form in a VORPAL input file since the code has a functional expression parser and can efficiently parse such mathematical expressions for evaluation at runtime. This allows us significant flexibility when designing photocathode simulations. For example, while the simulations presented here do not include a solenoidal field, it is straight forward to add such a field with only a few more lines in the input file. Simulations that include the effects of a solenoidal magnetic field are planned for the Phase II project. The parameters of the RF field are also listed in in Table 1.

We started in Phase I with simulations [1] of a Cu photocathode with a flat surface. Any algorithm refinements due to surface effects will be considered in Phase II. We used a laser pulse with a wavelength in the UV spectrum. The simulations presented here are with 266 nm wavelength. The physical parameters for a Cu cathode are given in Table 1. Notice that the energy of a photon for a laser pulse with wavelength of 266 nm is 4.66 eV. This is larger than the work function for Cu (4.6 eV). The simulations were run at strong RF fields ($E_0 = 50$ MV/m) which additionally decreases the effective barrier maximum at the surface.

We implemented the calculation of several beam diagnostics in post processing to gain understanding on the behavior of the implemented models. Specifically, we calculated the trace-space emittance (see, e.g. Ref. [34]), the rms bunch length, and rms beam radius as a function of the average (longitudinal) beam position [32, 33]. We provide the definitions of these quantities in one of the tasks for Phase II when we discuss the extensive verification of the models. The beam is generated from a Cu photocathode that is on the complete surface of the side $z = 0$ of the VORPAL simulation box and propagated in a $2\frac{1}{2}$ cell RF gun.

These results are consistent with previously published RF gun simulations with three different codes: ATRAP, ITACA, and PARMELA [32]. Our results reproduce all characteristics in the emittance, the rms beam radius, and the rms length even though the codes compared by Mouton *et al.* [32] had a beam emittance algorithm that is not based on any physics model for the photocathode (the beam was emitted according to a specified functional form, e.g. a cylindrical or a Gaussian beam shape) and were in cylindrical geometry. It is of considerable interest now to do a detailed, quantitative comparison of the photocathode models in VORPAL with other RF gun codes and, moreover, to validate the VORPAL code against experimental measurements. These problems will be addressed with Phase II tasks.

Finally, visualization of the RF gun simulations is essential to gain insight on how the modeled physical system evolves as well as to understand how the developed code behaves during runtime execution. We developed a very quick and basic visualization code to look at the emission of electrons from the photocathode. It is written in Python using the Gnuplot program and HDF5 libraries to access the raw VORPAL output data. Four snapshots of emitted electrons

[1] All simulations we did for the work in this task were run in parallel on the Tech-X Linux Cluster. These are 3D simulations of photocathode emission that are now feasible only on multi-processor systems with giga bytes of RAM. Results from this work will also be presented at the 2005 Particle Accelerator Conference (PAC2005).

(shown with white dots) during the interaction of the laser pulse with the photocathode are shown in Figs. 7 and 8. The ranges of the axes on each plot are determined by the minimum and maximum values of the particle coordinates since we wanted to focus only on the emitted beam. The actual simulation box is much larger. Its sizes are given in Table 1. The first plot is after the initial part of the pulse has interacted with the photocathode and the electron beam starts to leave the photocathode. The next two plots show the formation of the beam at two later times, correctly following the shape of the striking Gaussian beam. The last plot shows the completely emitted beam. We used such images to produce dynamically evolving diagnostics of the beam propagating in the photocathode (movies of the simulations particle data).

However, while this visualization approach was of considerable help to during the Phase I work, it is not sufficient to look at more advanced beam characteristics such as tracking beam particles that are emitted from different regions of the photocathode and how they affect the beam emittance. In a more realistic photocathode, e.g. a dispenser cathode with surface effects taken into account, different regions of the photocathode surface will have different work functions and will emit different amounts of charge. Even in the case we simulated here, photocathode regions see different laser intensity and emit different amounts of charge. It becomes important to understand how the formation and evolution of the beam in the RF gun in such cases influence the emittance.

We propose to implement the particle tracking visualization in the Phase II project and add this capability to the VORPAL code framework. Also, we have already been asked to provide particle tracking by VORPAL users in the Lawrence Berkeley National Lab for visualization of particle trapping when simulating advanced accelerator concepts in the case of propagating laser pulses in preformed or tunnel-ionized plasma channels.

The results presented for the Phase I tasks prove the feasibility of the proposed project and demonstrate how important it is to model the physics of photocathodes with high fidelity in order to produce experimentally high-quality beams. Moreover, we think that the work that we did in Phase I is a solid foundation for the development of a complete prototype for these models in Phase II and providing these new capabilities to researchers in the field.

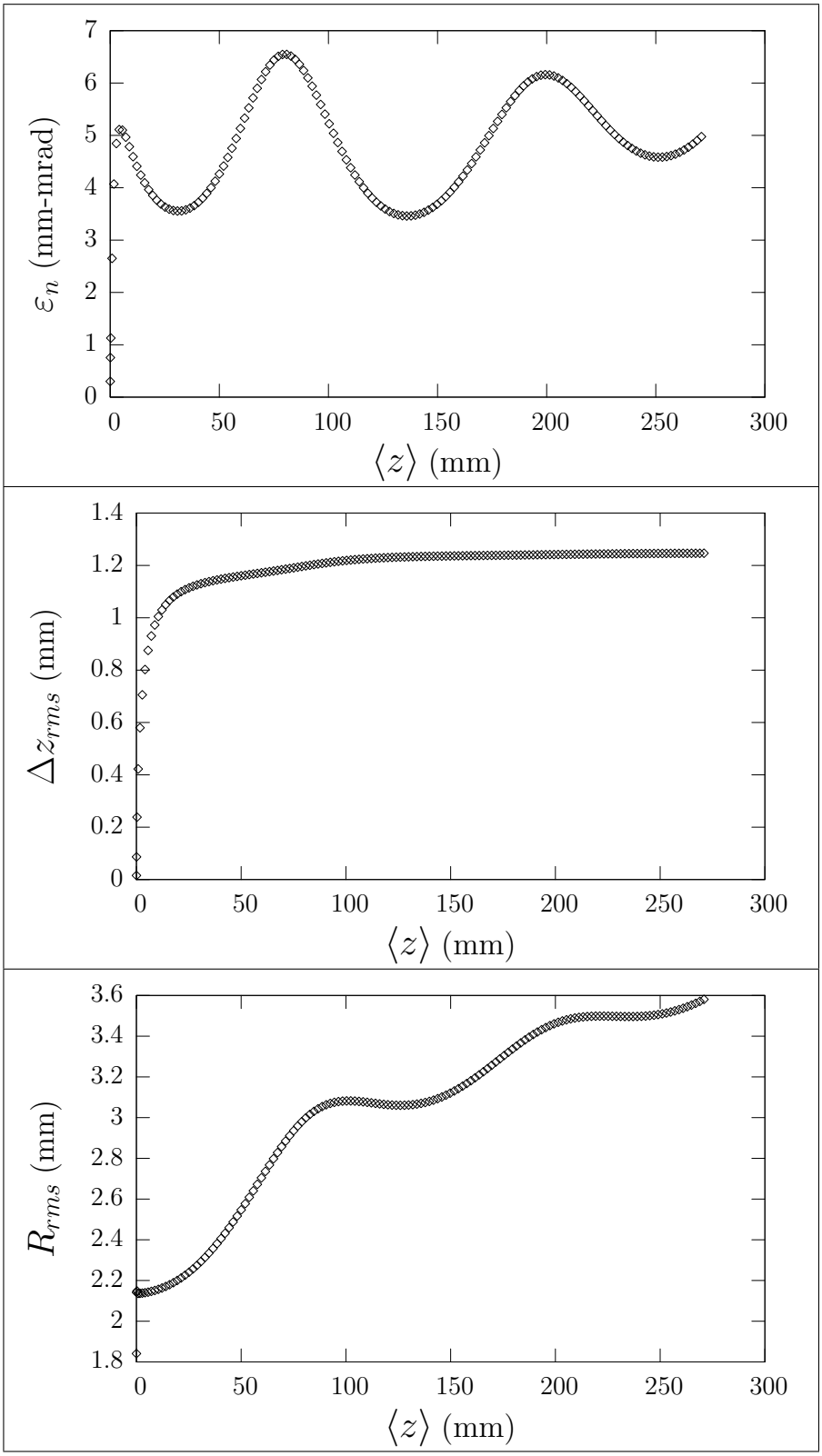

Figure 6: Beam rms diagnostics vs the average beam position from VORPAL simulations using the algorithm for the steady state model. The top plot shows the trace-space emittance, the middle one is the variation of the rms bunch length while the bottom panel represents the evolution of the rms beam radius. The beam is generated from a Cu photocathode in a $2\frac{1}{2}$ cell RF gun.

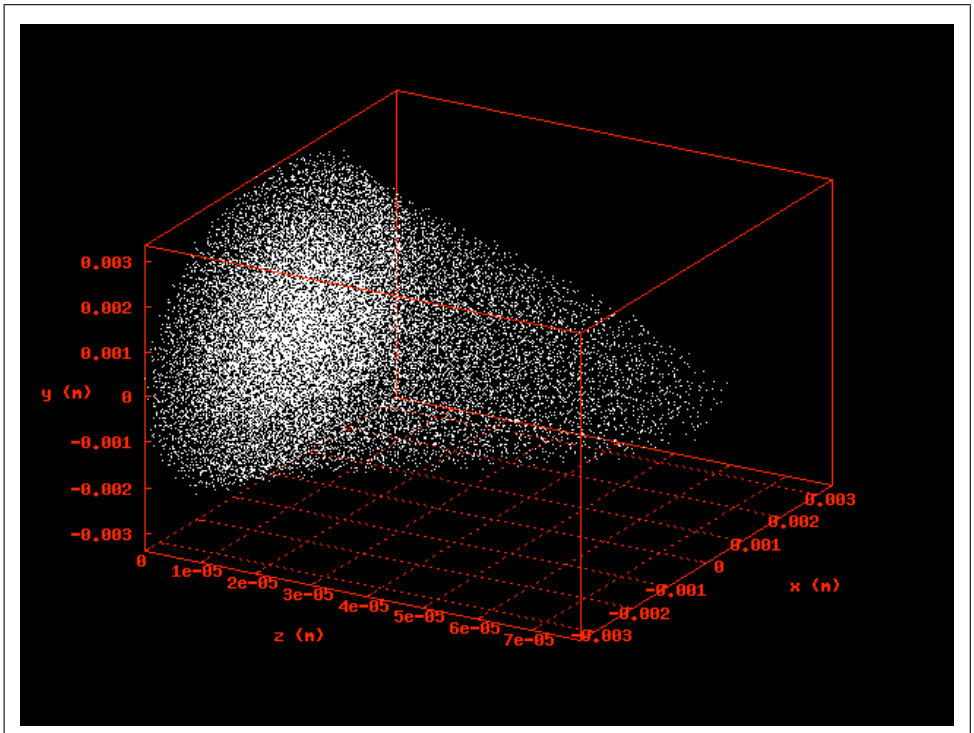

$t \approx 6.3$ ps, $N_t = 54$

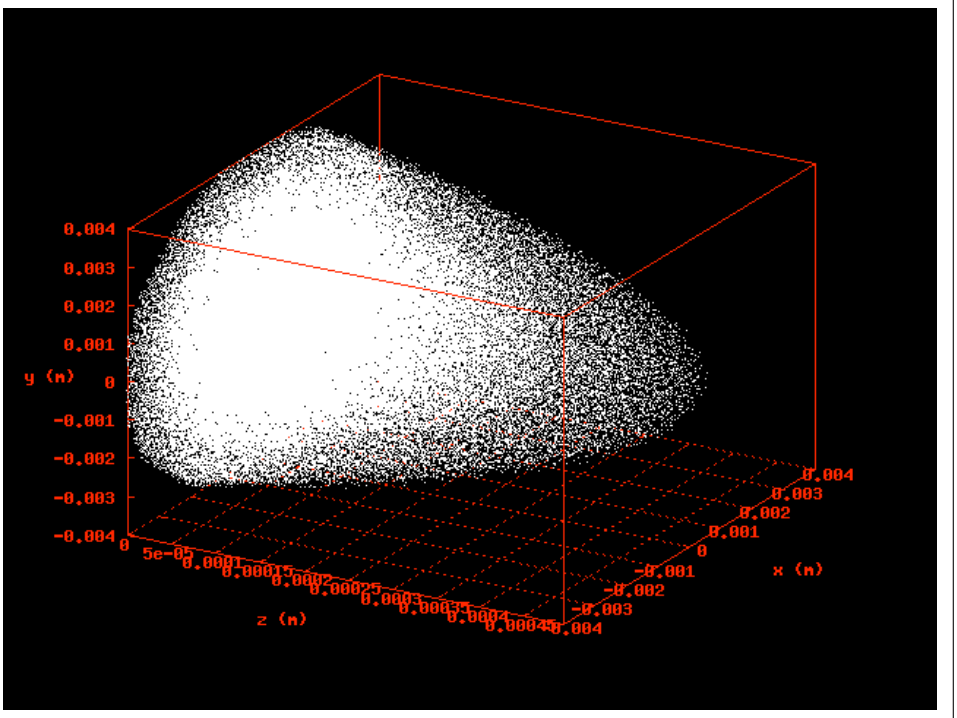

$t \approx 12.6$ ps, $N_t = 108$

Figure 7: Visualization diagnostic for the electron beam emittance and propagation in 3D RF gun simulations with VORPAL.

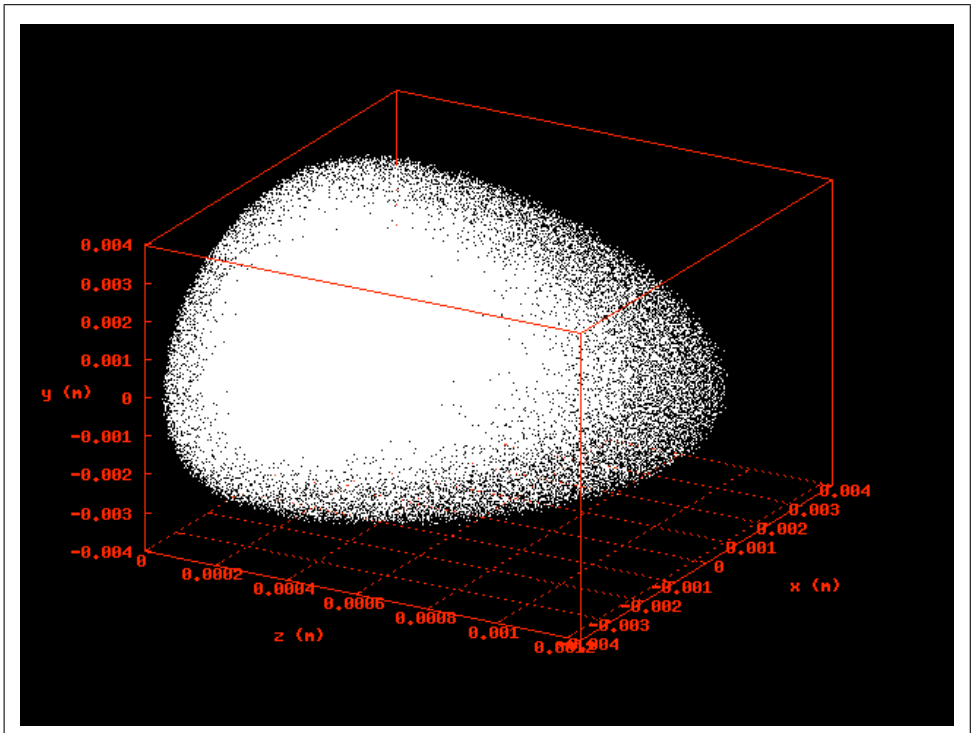

$t \approx 18.9$ ps, $N_t = 162$

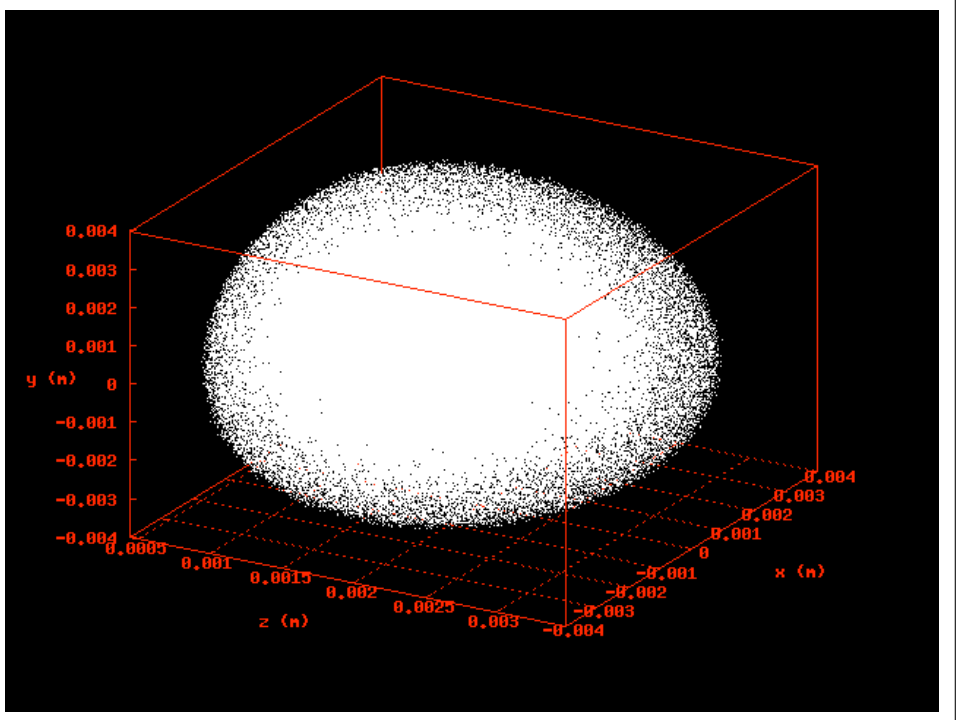

$t \approx 31.5$ ps, $N_t = 270$

Figure 8: Visualization diagnostic for the electron beam emittance and propagation in 3D RF gun simulations with VORPAL.

References

[1] The official source of information about the Next Linear Collider project can be accessed via the URL: "http://www-project.slac.stanford.edu/nlc/home.html".

[2] Information about the NCL injector systems research is available at the web page: "http://www-project.slac.stanford.edu/lc/local/systems/Injector/Injecto% rHomePage.html".

[3] See e.g. the web page of the Polarized Photocathode Research Collaboration at the URL "http://www.slac.stanford.edu/grp/rd/pprc/".

[4] "http://www-beams.colorado.edu/~cary/vorpaldocs/".

[5] J. R. Cary and C. Nieter. Vorpal: a arbitrary dimensional hybrid code for computation of pulse propagation in laser-based advanced acceleration concepts. In *18th Annual Review of Progress in Applied Computational Electromagnetics ACES 2002 (Monterey, CA)*, pages 549–555, 2002.

[6] C. Nieter and J. R. Cary. Vorpal: a versatile plasma simulation code. *J. Comput. Phys.*, 196:448–473, 2004.

[7] P. G. O'Shea and H. P. Freund. Free-electron lasers: Status and applications. *Science*, 292:1853–1858, 2001.

[8] D. H. Dowell *et al.* Slice emittance measurements at the SLAC Test Gun Facility. SLAC technical publication SLAC-PUB-9540 (2002) available online: "http://www.slac.stanford.edu/pubs/slacpubs/9000/slac-pub-9540.html".

[9] D. T. Palmer. The ORION photoinjector. In proceedings of the 2nd ORION Workshop (2003), "http://www-conf.slac.stanford.edu/orion/PAPERS/A05.PDF". See also the SLAC technical note publication: "http://www.slac.stanford.edu/grp/arb/tn/arbvol4/ARDB302.pdf".

[10] "http://www-conf.slac.stanford.edu/orion/".

[11] K. L. Jensen. Theory of field emission. In W. Zhu, editor, *Vacuum Microelectronics*, chapter 3. Wiley Interscience, New York, 2001.

[12] K. L. Jensen, P. G. O'Shea, and D. W. Feldman. Generalized electron emission model for field, thermal, and photoemission. *Appl. Phys. Lett.*, 81:3867–3869, 2002.

[13] N. A. Papadogiannis, S. D. Moustaïzis, and J. P. Girardeau-Montaut. Electron relaxation phenomena on a copper surface via nonlinear ultrashort single-photon photoelectric emission. *J. Phys. D*, 30:2389–2396, 1997.

[14] N. A. Papadigiannis and S. D. Moustaizis. Ultrashort laser-induced electron photoemission: a method to characterize metallic photocathodes. *J. Phys. D.*, 34:499–505, 2001.

[15] K. L. Jensen, D. W. Feldman, M. Virgo, and P. G. O'Shea. Measurement and analysis of thermal photoemission from a dispenser cathode. *Phys. Rev. ST Accel. Beams*, 6:083501–1/14, 2003.

[16] K. L. Jensen, D. W. Feldman, and P. G. O'Shea. Advanced photocathode simulation and theory. *Nucl. Instrum. & Methods Phys. Res. Sect. A, available online at "http://www.sciencedirect.com"*, 2003.

[17] C. K. Birdsall and A. B. Langdon. *Plasma Physics via Computer Simulation*. McGraw-Hill, New York, 1985.

[18] R. W. Hockney and J. W. Eastwood. *Computer Simulation Using Particles*. McGraw-Hill, New York, 1981.

[19] J. P. Verboncoeur, M. V. Alves, V. Vahedi, and C. K. Birdsall. Simultaneous potential and circuit solution for 1d bounded plasma particle simulation codes. *Journal of Computational Physics*, 104:321–328, 1993.

[20] V. Vahedi and M. Surendra. A monte carlo collision model for the particle-in-cell method: applications to argon and oxygen discharges. *Comp. Phys. Comm.*, 87:179–198, 1995.

[21] D. L. Bruhwiler, S. G. Shasharina, and J. R. Cary. The optsolve++ software components for nonlinear optimization and root-finding. In *Computing in Object Oriented Parallel Environments*, volume 1732 of *Lecture Notes in Computer Science*, pages 154–163, 1999.

[22] "`http://www.techxhome.com/products/optsolve/`".

[23] "`http://hdf.ncsa.uiuc.edu/HDF5/`".

[24] C. G. R. Geddes, C. Toth, J. van Tilborg, E. Esarey, C. B. Schroeder, W. P. Leemans, D. Bruhwiler, C. Nieter, and J. Cary. High quality electron beams from a plasma channnel guided laser wakefield accelerator. submitted for publication.

[25] C. B. Laney. *Computational Gas Dynamics*. Cambridge University Press, Cambridge, United Kingdom, 1998.

[26] G. A. Sod. A survey of several finite-difference methods for systems of nonlinear hyperbolic conservation laws. *J. Comput. Phys.*, 27:1–31, 1978.

[27] K. L. Jensen, D. W. Feldman, N. Moody, and P. G. O'Shea. A photoemission model for low work function coated metal surfaces and its experimental validation. submitted for publication, (2005).

[28] S. I. Anisimov, B. L. Kapeliovich, and T. L. Perelman. *Sov. Phys. JETP*, 39:375, 1974.

[29] V. S. Vladimirov. *Equations of Mathematical Physics*. Mir Publishers, Moscow, 1984.

[30] L. W. Johnson and R. D. Riess. *Numerical Analysis*. Addison-Wesley, second edition, 1982.

[31] W. H. Press, S. A. Teukolsky, W. T. Vetterling, and B. P. Flannery. *Numerical Recipes in C: The Art of Scientific Computing*. Cambridge University Press, second edition, 1992.

[32] B. Mouton, J. L. Coacolo, and L. Serafini. Code comparison in rf-gun simulations. In S. Myers *et al.*, editor, *EPAC 96: Fifth European Particle Accelerator Conference*, page 1283. American Institute of Physics, 1996.

[33] E. Colby, V. Ivanov, Z. Li, and C. Limborg. Simulation issues for rf photoinjectors. In *International Computational Accelerator Physics Conference (ICAP 2002), Michigan State University, October 15-18th.2002*. American Institute of Physics.

[34] K. Floettmann. Some basic features of the beam emittance. *Phys. Rev. ST Accel. Beams*, 6:034202–1/7, 2003.